

Article

The Critical Behaviour and Magnetism of MnCoGe_{0.97}Al_{0.03} Compounds

Abdul Rashid Abdul Rahman ^{1,*}, Muhamad Faiz Md Din ^{1,2,*}, Norinsan Kamil Othman ³, Jianli Wang ^{2,4}, Nur Sabrina Suhaimi ¹, Shi Xue Dou ², Noor Fadzilah Mohamed Sharif ¹ and Nazrul Fariq Makmor ¹

¹ Department of Electrical & Electronic Engineering, Faculty of Engineering, National Defence University of Malaysia, Kuala Lumpur 57000, Malaysia; sabrina15.eec@gmail.com (N.S.S.); noorfadzilah@upnm.edu.my (N.F.M.S.); nazrulfariq@upnm.edu.my (N.F.M.)

² Institute for Superconductivity and Electronic Materials, University of Wollongong, Wollongong, NSW 2522, Australia; jianliwang@jlu.edu.cn (J.W.); shi_dou@uow.edu.au (S.X.D.)

³ Department of Applied Physics, Faculty of Science and Technology, The National University of Malaysia, 43600 UKM, Bangi 43600, Malaysia; insan@ukm.edu.my

⁴ College of Physics, Jilin University, Changchun 130012, China

* Correspondence: rashidrahman2201@gmail.com (A.R.A.R.); faizmd@upnm.edu.my (M.F.M.D.)

Abstract: The critical behaviour associated with the field-induced martensitic transformation heavily relies on the vacancy and transition of the magnetic phase in MnCoGe based-compounds. Due to this revelation, an intensive investigation was brought forth to study the substitution of Ge (atomic radius = 1.23 Å) by Al (atomic radius = 1.43 Å) in MnCoGe_{0.97}Al_{0.03} alloy compound. The room-temperature X-ray diffraction indicated that the reflections were identified with the orthorhombic structure (TiNiSi-type, space group Pnma) and minor hexagonal structure (Ni₂In-type, space group P₆₃/mmc). The substitution of Al in the supersession of Ge transmuted the crystal structure from TiNiSi-type to Ni₂In-type structure. The MnCoGe_{0.97}Al_{0.03} compound's magnetism was driven by interactions that are long in range, as indicated by the study of the critical behaviour in the proximity of T_C. The magnetic measurement and neutron diffraction revealed that the structural transition took place with the decrease in temperature. The results from neutron diffraction signify that the transformation of the magnetic field-induced martensitic has a crucial function in producing the immense effect of magnetocaloric systems such as these. This outcome serves a critical function for investigations in the future.

Keywords: critical behaviour; magnetocaloric effect; second-order magnetic transition; long-range interactions; magnetic refrigeration



Citation: Rahman, A.R.A.; Md Din, M.F.; Othman, N.K.; Wang, J.; Suhaimi, N.S.; Dou, S.X.; Mohamed Sharif, N.F.; Makmor, N.F. The Critical Behaviour and Magnetism of MnCoGe_{0.97}Al_{0.03} Compounds. *Crystals* **2022**, *12*, 205. <https://doi.org/10.3390/cryst12020205>

Academic Editor: Charles Rosenblatt

Received: 31 December 2021

Accepted: 27 January 2022

Published: 29 January 2022

Publisher's Note: MDPI stays neutral with regard to jurisdictional claims in published maps and institutional affiliations.



Copyright: © 2022 by the authors. Licensee MDPI, Basel, Switzerland. This article is an open access article distributed under the terms and conditions of the Creative Commons Attribution (CC BY) license (<https://creativecommons.org/licenses/by/4.0/>).

1. Introduction

The magnetocaloric effect (MCE) is a fundamental magneto-thermal phenomenon known as the cooling or warming of magnetic material in adiabatic conditions due to a change in the applied magnetic field [1]. Weiss and Piccard first discovered this phenomenon in nickel in 1917 [2,3]. Many materials have been examined with magnetic cooling in mind. Interest increased significantly with discovering the giant magnetocaloric effect in Gd during the 1970s to 1990s [4,5]. A great many material families with second-order magnetic phase transitions have been studied for the application of the magnetocaloric effect, such as rare earth and related alloys (e.g., [6–9]), Laves phases RT₂ (e.g., [1,10,11]), rare-earth manganites (e.g., [10–12]), RT₂ × 2 compounds (X: Si or Ge) (e.g., [13–16]) and MM'X alloys (M and M' denote 3d transition elements and X denotes main group elements) [17–20].

The MnCoGe based alloy is a group of the MM'X family with good physical properties and promising application potential. It has two crystalline structures, TiNiSi-type orthorhombic structure and Ni₂In-type hexagonal structure [21]. It was previously found that MnCoGe_{1-x}Al_x offers the best ability to control the temperature window [22]. This is

important in investigating entropy changes' structural and magnetic transition effects in giant magnetocaloric effect (GMCE) materials. In addition, the field-induced manner can investigate the martensitic transformation of the GMCE materials.

This work has instigated the critical exponent analysis of $\text{MnCoGe}_{0.97}\text{Al}_{0.03}$ compounds in the ferromagnetic (FM) region to paramagnetic (PM) ordering. The analysis was conducted to better understand the behaviour of the physical quantities of near-continuous phase transitions in $\text{MnCoGe}_{0.97}\text{Al}_{0.03}$. The scaling hypothesis theorizes that a second-order transition near T_C is characterized by a set of critical exponents, namely β , γ , and δ [23]. The critical properties of $\text{MnCoGe}_{0.97}\text{Al}_{0.03}$ alloy around the ferromagnetic to paramagnetic phase transition were investigated through various methods: the modified Arrott plots (MAP), the Kouvel–Fisher method, and the critical isotherm analysis. The study effectively shifted the magnetic phase transition and structural change into the temperature region of interest, contributing to a GMCE. In addition, the strong reliance on proper tuning for the phase transition critical behaviour served as a point of reference for a fascinating discovery concerning the replacement for Ge (1.37 Å atomic radius) by Al (1.43 Å atomic radius) in $\text{MnCoGe}_{0.97}\text{Al}_{0.03}$ compounds. The tuning dependency was caused by magnetic and structural transition voids and a field-induced martensitic transformation. Results demonstrated that the sample exhibited a structural transition at a temperature of 420 K and a second-order FM–PM transition at a temperature of 352 K. Lastly, neutron diffraction with a temperature-dependent experiment was conducted to confirm the coupling of the magnetic phase transition and the structural transition.

2. Materials and Methods

In preparing the batch of $\text{MnCoGe}_{0.97}\text{Al}_{0.03}$ compounds, suitable amounts of Mn (99.9%), Ge (99.99%) powder, Co (99.9%), and Al (99.9%) chips were arc-melted under an argon atmosphere. About 3% of Mn above the stoichiometric amount was required of the starting materials. This is required for evaporation to compensate for lost weight during the melting procedure. In attaining good homogeneity of the samples, the ingots were melted 5 times consecutively. After that, they were closed in an evacuated quartz tube and toughened at a temperature of 900 °C for 120 h. In characterizing the samples, they were then put under the X-ray diffraction (XRD) (Cu K α radiation, $\lambda = 1.5418$ Å) and differential scanning calorimetry (DSC) measuring devices at the room temperature. A 14 T physical property measurement system (Quantum Design) was used to measure the magnetization using its vibrating sample magnetometer option. This was performed at a 10–600 K temperature range and up to 5 T of applied fields. The Wombat high-intensity powder diffractometer was used to collect the neutron data at a 5–340 K temperature range with an incident neutron wavelength of $\lambda = 2.4205$ Å located at the Open Pool Australia Lightwater (OPAL) reactor.

3. Results

3.1. Structure Properties

Figure 1 shows the X-ray diffraction (XRD) patterns of $\text{MnCoGe}_{0.97}\text{Al}_{0.03}$ at room temperature. The peaks were identified with primary TiNiSi-type structure (orthorhombic; space group $Pnma$) and minor Ni_2In -type structure (hexagonal, space group $P63/mmc$). The change in crystal structure was noticeable with the Al substitution for Ge atoms. As shown by the refinement analysis, the $\text{MnCoGe}_{0.97}\text{Al}_{0.03}$ pattern exhibited an orthorhombic TiNiSi-type structure that has a mix of a minuscule number of 4 ± 0.2 wt % of hexagonal phase. The results suggest that with the Al-doping, there was also an increase in the fraction of hexagonal austenite at room temperature. This means there was a tendency to maintain the Ni_2In -type austenite and lower the T_{str} value by employing Al substitution for Ge.

3.2. Magnetic Phase Transitions

Temperature dependence of magnetization (M–T curves) with the influence of 0.01 T low-field and differential scanning calorimetry measurement (DSC) of $\text{MnCoGe}_{0.97}\text{Al}_{0.03}$ compounds was conducted in the 10–600 K range to determine the transition temperature,

as depicted in Figure 2. The FM to PM transition temperature is defined as the one in which the largest slope occurs, as depicted in the inset of Figure 2a. The Curie temperature (T_C) is $T_C = 342$ at MnCoGe and $T_C = 352$ at MnCoGe_{0.97}Al_{0.03}. The T_C increased with Al doping, which implies that the exchange interaction among the magnetic atom became stronger with the Al substitution [24]. The DSC measurement revealed a slight drop in the structural transition temperature from $T_{str} \approx 450$ K (MnCoGe) to $T_{str} \approx 420$ K (MnCoGe_{0.97}Al_{0.03}). The maxima of the DSC signals were used to determine the transition temperature values. These values coincided with the magnetization measurements, which agreed well with the DSC measurements. This behaviour shows that the MnCoGe-based compounds underwent a structural transition driven by replacing the Ge with Al, hence changing the temperature when cooled to a lower temperature.

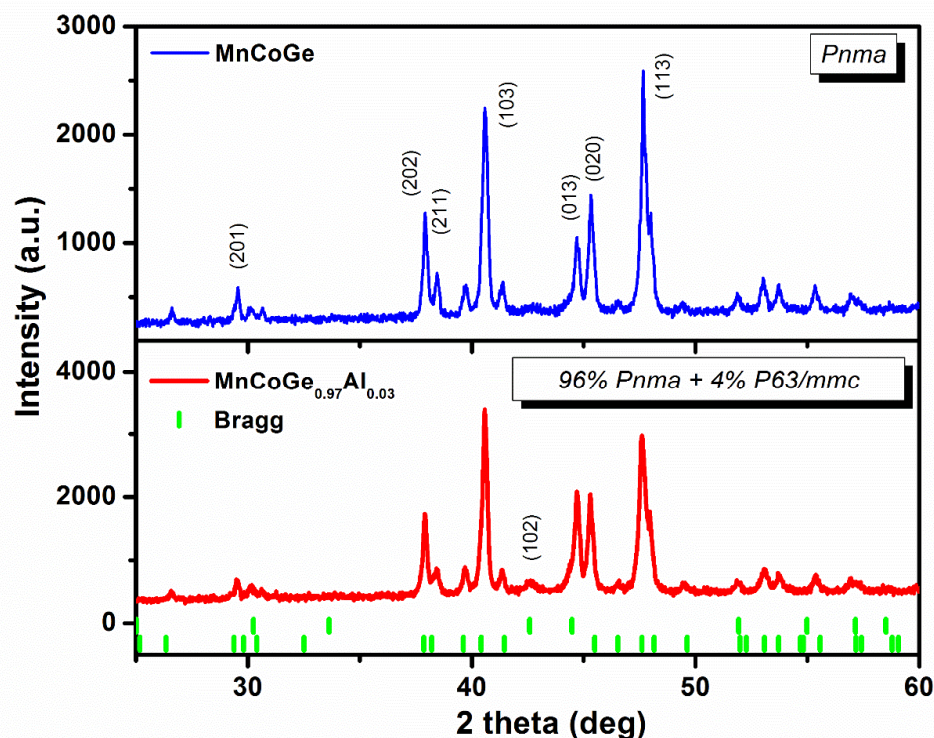


Figure 1. Measured MnCoGe and MnCoGe_{0.97}Al_{0.03} powder XRD patterns at room temperature. The typical hexagonal Ni₂In-type (**top**) and orthorhombic TiNiSi-type (**bottom**) structures are denoted by the Miller indices (hkl).

3.3. Critical Exponent Analysis

The critical behaviour was analyzed near the T_C value for the MnCoGe_{0.97}Al_{0.03} compound to further define the transition behaviour of the FM-PM phase. Figure 3 shows the measured isothermal magnetization against the applied field around T_C at 4 K and 2 K intervals. The isotherm plot determines the magnetic transition order according to the proposed criterion outlined by Banerjee [25]. Figure 4 shows the standard Arrott plot of B/M versus M^2 at temperatures close to T_C . A negative slope of the B/M versus M^2 curves indicates a first-order transition, while a positive slope shows a second-order transition. Second-order phase transition is observed during the transition temperature range when there is a constant positive slope of the B/M for the MnCoGe_{0.97}Al_{0.03} compound. The consistency with the magnetic and thermal hysteresis near the PM of the results is confirmed by the second-order transition's nature. A second-order magnetic phase transition near T_C that is described by critical exponents such as β , γ , and δ was suggested by the scaling hypothesis [23].

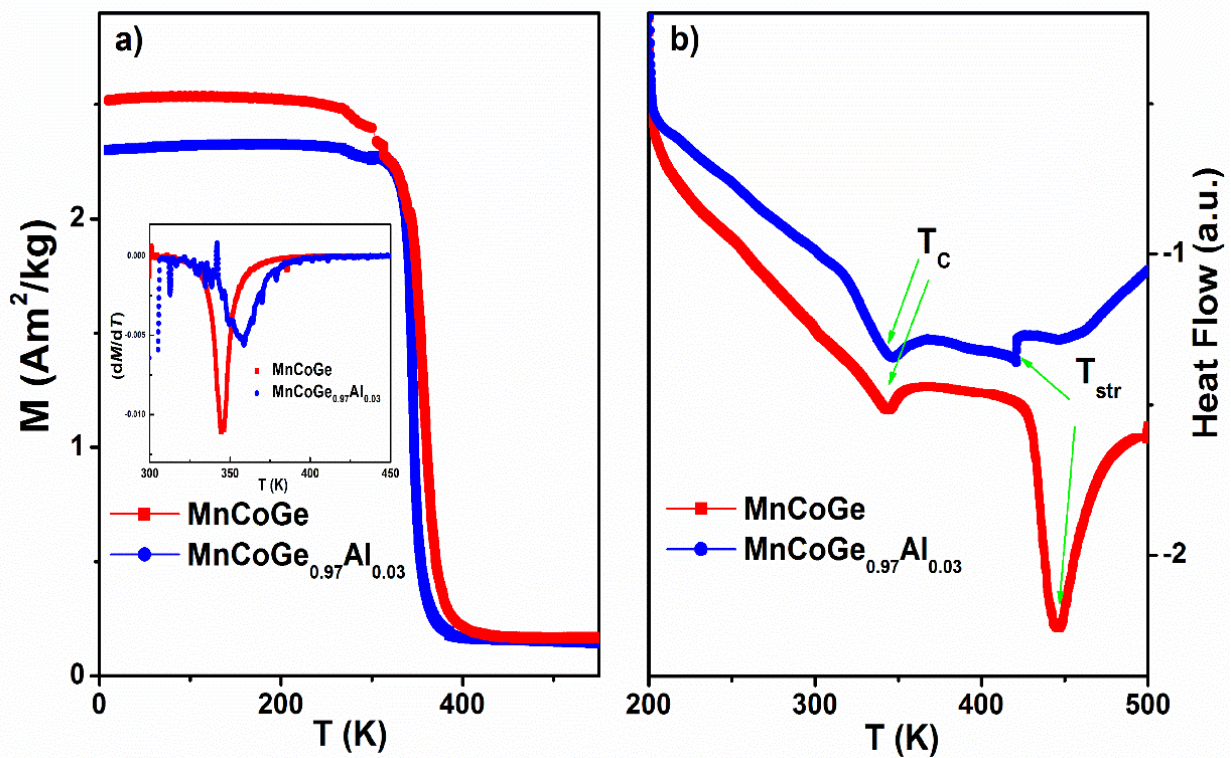


Figure 2. (a) M-T curves for $\text{MnCoGe}_{0.97}\text{Al}_{0.03}$ measured with a 0.01 T magnetic field. (b) DSC curves measured within the range of 200–500 K. The arrows indicate the Curie temperature and the structural transition of the compounds.

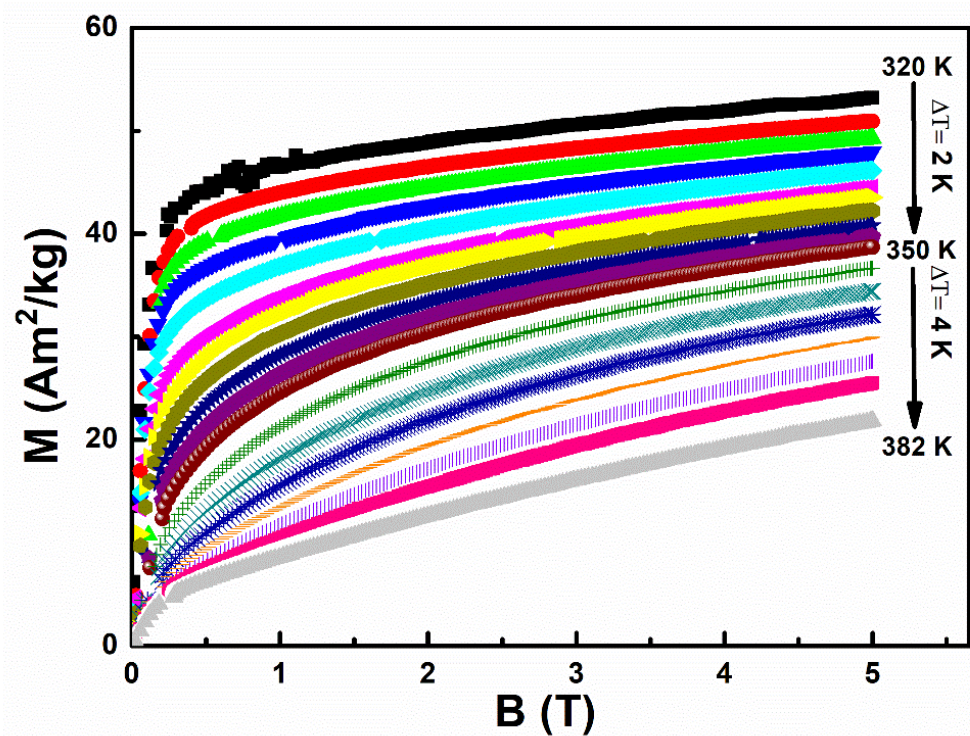


Figure 3. $\text{MnCoGe}_{0.97}\text{Al}_{0.03}$ compound isothermal magnetization curves in the T_C vicinity.

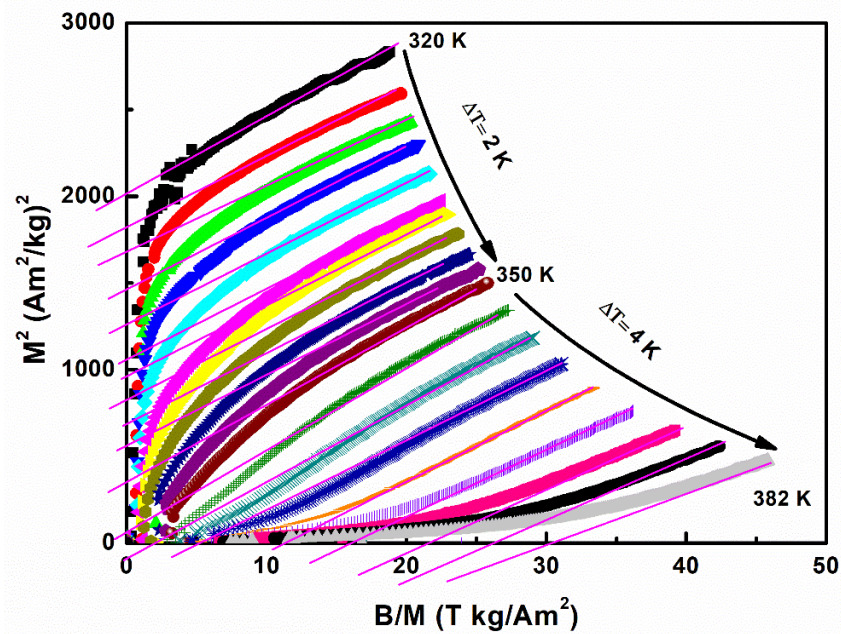


Figure 4. MnCoGe_{0.97}Al_{0.03} compound Arrott plots (M^2 vs. B/M) at temperatures within the T_C area.

Several methods were employed to study the critical behaviour of the MnCoGe_{0.97}Al_{0.03} compound, such as the modified Arrott plots (MAPs), critical isotherm analysis, Widom scaling relation, and the Kouvel–Fisher method. The MAPs method was the first to compute the critical components derived by the Arrott–Noakes state equation [23]. The following equations were used to make quantitative fits to the Arrott plots [26].

$$M_S(T) = \lim_{(H \rightarrow 0)}(M) = M_0(-\varepsilon)^\beta, \varepsilon < 0 \quad (1)$$

$$\chi_0^{-1}(T) = \lim_{(H \rightarrow 0)}\left(\frac{H}{M}\right) = \left(\frac{h_0}{M_0}\right)\varepsilon^\gamma, \varepsilon > 0 \quad (2)$$

In the equations, the reduced temperature ($= (T - T_C)/T_C$) is given by ε while M_0 and h_0 parameters are constant. β and γ initial values were chosen before the plot of $M^{1/\beta}$ versus $(B/M)^{1/\gamma}$ where the linearly extrapolated curve intersection with the $M^{1/\beta}$ axis is then obtained. This was done to determine the spontaneous magnetization, M_S . The mutually misaligned magnetic domains tend to cause linearity deviation of the MAPs at low fields. Thus, it should be critical that only the linear region of the high field is used [27].

Next, the $M_S(T, 0)$ against temperature $\chi_0^{-1}(T, 0)$ was plotted and fitted using Equations (1) and (2), as shown in Figure 5. New MAPs were then constructed using the new critical exponent values. Critical parameters of $\gamma = 0.80$ and $\beta = 0.429$ were yielded by the MAPs shown in Figure 6 using Equations (1) and (2).

The critical exponents β and γ can be determined more accurately by using the Kouvel–Fisher (KF) method [27] using Equations (3) and (4) as depicted below:

$$\frac{M_S(T)}{\frac{dM_S(T)}{dT}} = \frac{T - T_C}{\beta} \quad (3)$$

$$\frac{\chi_0^{-1}(T)}{d\chi_0^{-1}(T)dT} = \frac{T - T_C}{\gamma} \quad (4)$$

As can be seen in Figure 7 and according to Equations (3) and (4), slopes of $1/\beta$ and $1/\gamma$ can be achieved by plotting $M_S(T) \left[\frac{dM_S}{dT}\right]^{-1}$ and $\chi_0^{-1}(T) \left[\frac{d\chi_0^{-1}}{dT}\right]^{-1}$ against temperature. The interception of the lines on the x-axis was used to obtain the T_C value. The Kouvel–

Fisher method was used to obtain the following parameters of critical exponents and T_C : $\beta = 0.44$; $\gamma = 0.83$; $\delta = 2.89$; and $T_C = 352$ K. The MAPs were utilized to calculate the β and γ : critical exponents. The values from the KF method match well with the values obtained using the MAPs method when a comparison is made. The critical isotherm $M(T_C, H)$ can directly determine the critical component δ value based on Equation (5):

$$M_{T_C} = DH^{\frac{1}{\delta}}, \quad \varepsilon = 0, T = T_C \tag{5}$$

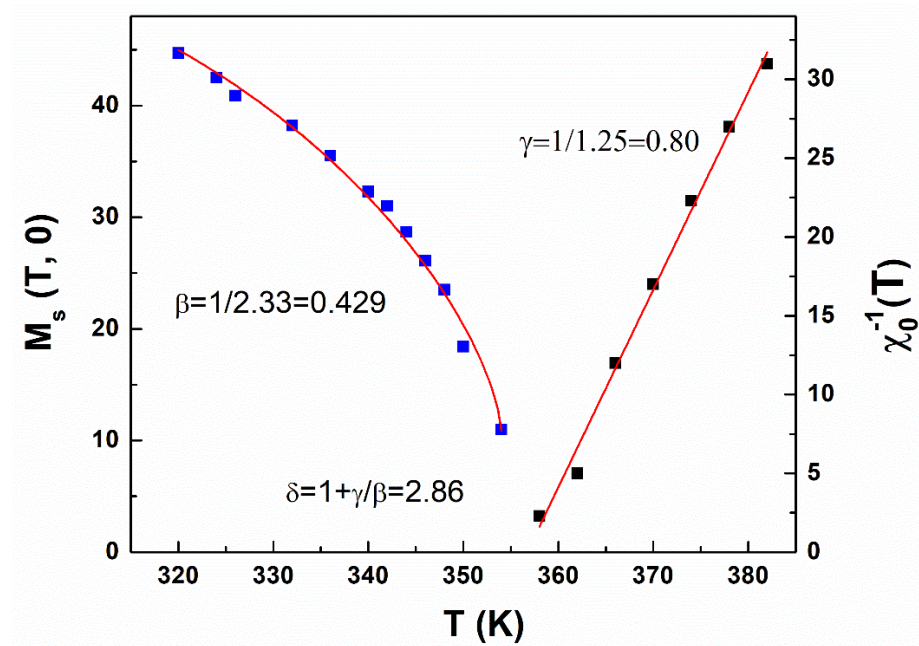


Figure 5. Temperature dependence of the spontaneous magnetization $M_S(T, 0)$ and the inverse initial susceptibility $\chi_0^{-1}(T, 0)$.

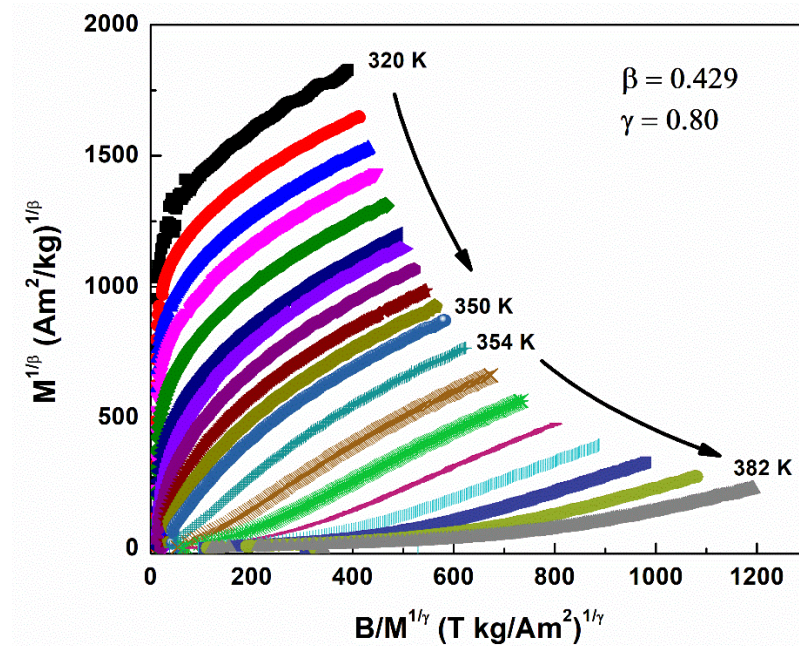


Figure 6. Modified Arrott plot: isotherms of $M^{1/\beta}$ vs. $(B/M)^{1/\gamma}$ with the calculated exponents $\beta = 0.429$ and $\gamma = 0.80$.

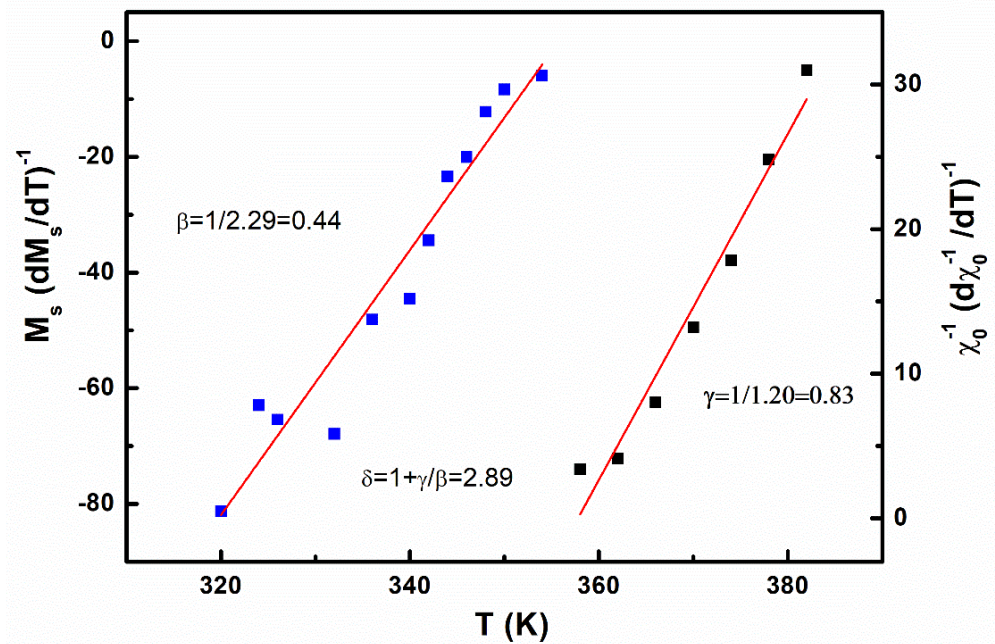


Figure 7. Kouvel-Fisher plot for the spontaneous magnetization $M_S(T)$ and the inverse initial susceptibility $\chi_0^{-1}(T)$. Solid lines are fitted to Equations (3) and (4).

The Widom scaling relation is an alternative in obtaining the critical exponent δ . This can be seen in Equation (6):

$$\delta = 1 + \gamma/\beta \quad (6)$$

The MAPs and Kouvel–Fisher methods were employed to obtain the critical parameters β and γ . By combining the critical parameters with Equation (5), the δ values were deduced to be 2.89 and 2.86, separately. Hence, the experimental data that were used to deduce the critical exponent confirmed its reliability using the Widom scaling relation. The scaling theory can be used to confirm the reliability of the exponents β and γ that were calculated. According to the scaling theory in the critical region, the state magnetic equation can be expressed as:

$$M(H, \varepsilon) = \varepsilon^\beta f_\pm \left(\frac{H}{\varepsilon^{\beta+\gamma}} \right) \quad (7)$$

where the reduced temperature is given by ε and the typical critical functions above and below T_C are given by $(T - T_C)/T_C$ and f_+ and f_- . The M/ε^β versus $H/\varepsilon^{(\beta+\gamma)}$ plots that can be seen in Figure 8 produced two universal curves from the β and γ values that were obtained by using the Kouvel–Fisher method: one curve for temperatures above and the other below the T_C , which agrees with the scaling theory. Hence, the acquired critical exponents and T_C values were confirmed to be reliable and agreed with the scaling hypothesis.

It is generally known that the phase transition's order parameter within the magnetic transition temperature fluctuates on all available length scales. The correlation in the continuous phase transition system's microscopic details is spread over by these fluctuations [28]. The critical behaviour of the $\text{MnCoGe}_{0.97}\text{Al}_{0.03}$ compound around T_C is dominated by long-range interactions in this compound, indicated by the closeness of the derived δ , β , and γ values to the mean-field values [29]. In the MnCoGe-based compound, the distance of Mn-Mn plays an important role in the magnetic transition. Thus, the competition between the localized Mn-Mn magnetic interactions should be responsible for the critical behaviour in the $\text{MnCoGe}_{0.97}\text{Al}_{0.03}$ compound as Al is diluted and does not contribute to the enhancement of the magnetic moment.

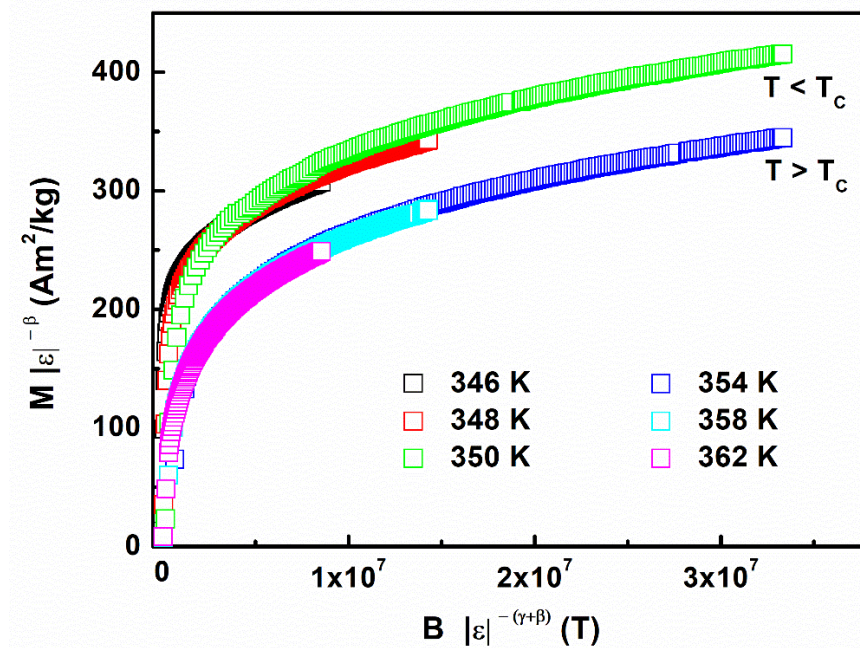


Figure 8. Universal curves by the scaling plots below and above T_C values for the $\text{MnCoGe}_{0.97}\text{Al}_{0.03}$ compound.

The isothermal magnetization near T_C determined the $\text{MnCoGe}_{0.97}\text{Al}_{0.03}$ compound's critical exponents. The critical isotherm analysis, Kouvel–Fisher method, and modified Arrott plots were among the various techniques this determination was based on. Additionally, all the critical exponents fulfilled the Widom scaling law criteria. The scaling Equation validates the calculated critical exponents with the acquired field, magnetization, and temperature data below and above T_C , showing two different curves' collapse. Hence, the calculated exponents were confirmed to be unambiguous and intrinsic. This was due to the magnetization data above and below T_C scaling acquired by different methods using their specific critical exponents' behaviour and the consistency in their values.

3.4. The Magnetocaloric Effect

The magnetization curves obtained for $\text{MnCoGe}_{0.97}\text{Al}_{0.03}$ ($B = 0\text{--}5$ T fields range) from the FM to the PM ordering temperatures are depicted in Figure 3. The decreasing and increasing fields' data at 2 K and 4 K intervals that span at the T_C range were obtained; as a result, evidence supporting the absence of magnetic hysteresis loss effects in second-order magnetic transitions was provided. Moreover, Figure 4 shows the corresponding Arrott plot (M^2 versus B/M), which displays second-order transition features. This was particularly confirmed by the lack of S-shaped Arrott plots close to the T_C and a positive sign of the coefficient $c^2(T)$ in the magnetic free energy Landau expansion [15].

The magnetic entropy change, $-\Delta S_M$, was determined for the $\text{MnCoGe}_{0.97}\text{Al}_{0.03}$ compound. This was performed by evaluating its magnetization curves for the increment and decrement field values within $\Delta B = 0\text{--}5$ T field range. The standard Maxwell relation was applied to derive the magnetic entropy change [30]:

$$-\Delta S_M(T, H) = \int_0^H \left(\frac{\partial M}{\partial T} \right)_H (dH) \quad (8)$$

With the uncertainty of using the first-order systems by Maxwell's relation, a method to define the first-order system's magnetic entropy change was achieved by Caron et al. using a decreasing field [31]. This case study used the decreasing field mode to evaluate the $-\Delta S_M$ magnetic entropy change. Figure 9 shows this by the closed symbol curves. There was no difference between the calculated $-\Delta S_M$ values of the increasing and decreasing

fields when a comparison was made. Thus, no hysteresis that occurs close to the magnetic transition is confirmed to be lost. The magnetic entropy change maximal value is around $4.93 \text{ J}\cdot\text{kg}^{-1}\text{K}^{-1}$ for $\text{MnCoGe}_{0.97}\text{Al}_{0.03}$ at 0–5 T field change.

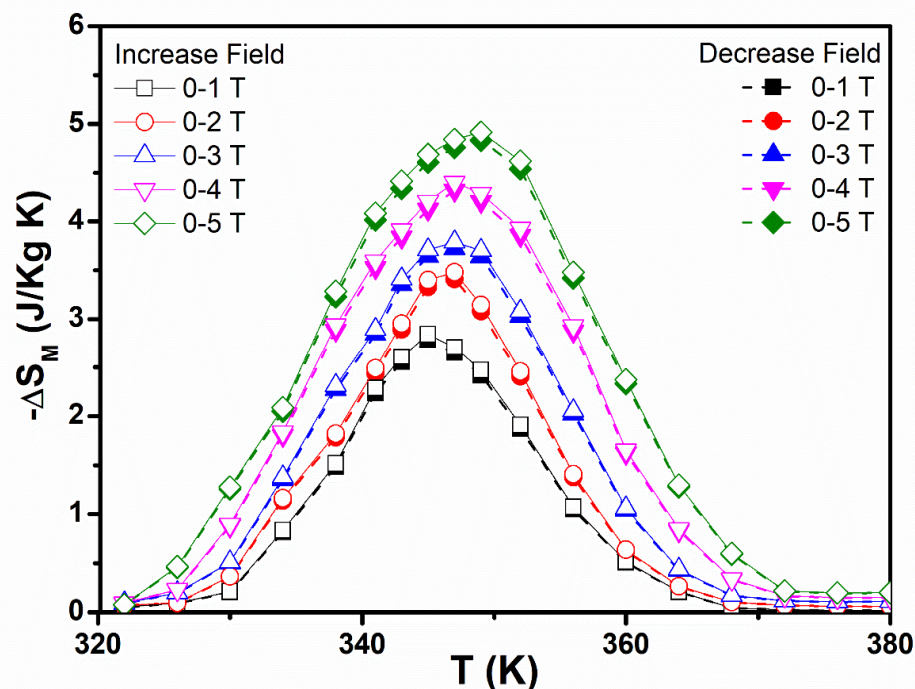


Figure 9. The isothermal magnetic entropy change, $-\Delta S_M(T, H)$ temperature dependence for $\text{MnCoGe}_{0.97}\text{Al}_{0.03}$ compounds calculated from magnetization isotherms with an applied field change of 0–5 T. Increasing fields are represented by open symbols while the decreasing fields are represented by closed symbols.

3.5. Neutron Diffraction

The neutron diffraction measurement contour plot of the $\text{MnCoGe}_{0.97}\text{Al}_{0.03}$ compound from 6 to 450 K is presented in Figure 10. The orthorhombic phase (space group $Pnma$) Miller indices (hkl) are not marked with the * symbol. The hexagonal-phase (space group $P63/mmc$) Miller indices (hkl) are marked with the * symbol. The decrease in temperature initiated a structural transition that started at a temperature of 430 K and ended at 350 K. The DSC and magnetic measurements coincided well. In addition, at around 420 K, a phase transition was revealed.

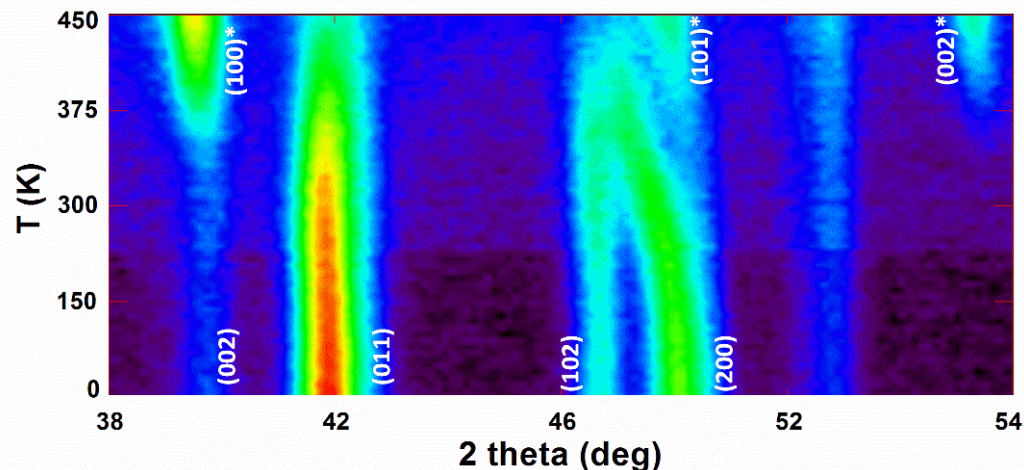


Figure 10. Neutron diffraction image for $\text{MnCoGe}_{0.97}\text{Al}_{0.03}$ collected at 6–450 K temperature range at 5 K steps over.

T_{str} was slightly reduced to ~ 420 K when Mn was substituted for a small amount of Al (3 wt %). This is different compared to its parent compound, MnCoGe, that had its structural change at $T_{str} \approx 450$ K. To investigate the crystallographic behaviour of the MnCoGe_{0.97}Al_{0.03} compound, the patterns of neutron diffraction were obtained at the chosen temperatures of $T = 6$ K, 300 K, 400 K, and 450 K, as in Figure 11. The neutron diffraction refinement patterns indicate that the compound crystallized into a hexagonal Ni₂In-type structure (space group *P63/mmc*) at 450 K. At a minimum temperature of 6 K, there was a total crystal structure change to TiNiSi-type orthorhombic structure (*Pnma*). At the temperatures of 400 K (40(2.86) % *Pnma* + 60(3.65) % *P63/mmc*) and 300 K (96.61(0.66) % *Pnma* + 3.39(13.98) % *P63/mmc*), both phases existed at once, validating the magnetic measurement expectations. Hence, based on the results, the stability of the hexagonal *P63/mmc* phase was improved by replacing Al for Ge.

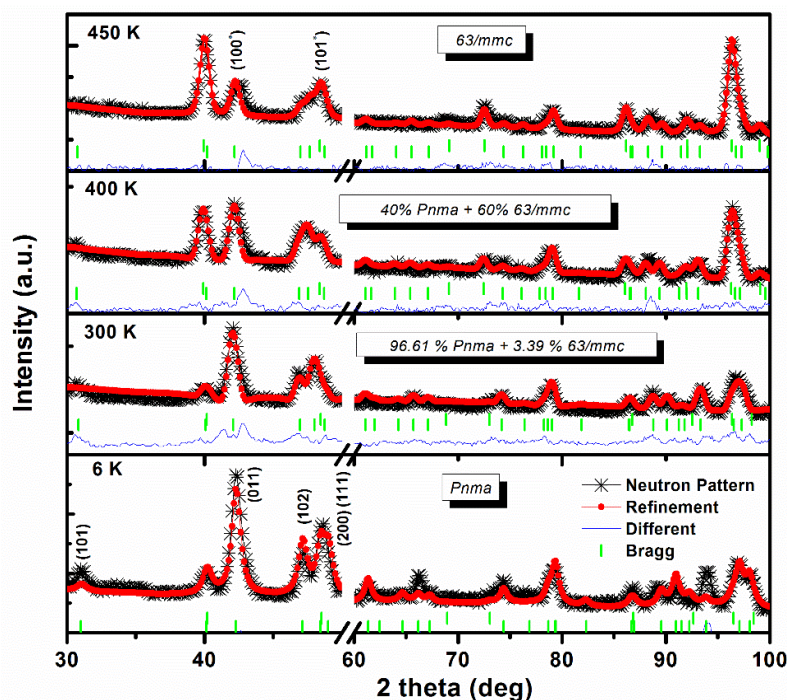


Figure 11. Neutron diffraction patterns for the MnCoGe_{0.97}Al_{0.03} compound measured at 6 K, 300 K, 400 K, and 450 K. The pattern with symbols represents the experimental data, while the calculated refinement data are expressed by the solid lines.

The neutron diffraction data were analyzed even further using the Rietveld refining method. This gave the output of the lattice parameters and the volume phase fractions: hexagonal and orthorhombic. Figure 12 shows the temperature against peak intensities of the reflections: (002)* (for *P63/mmc*); and (011) (for *Pnma*). The (011) reflection peak intensity decreased its value with temperature increase. The *Pnma* phase fraction decrement corresponds to this change. At the same time, the peak intensity of the (002)* value increased with temperature, which corresponds to the *P63/mmc* phase fraction increase with temperature. The structural parameters of the MnCoGe_{0.97}Al_{0.03} compound that were refined from the neutron diffraction data are represented as a function of temperature in Figure 13. The denotations $a = a_{ortho} = c_{hex}$, $b = b_{ortho} = a_{hex}$, $c = c_{ortho} = \sqrt{3}a_{hex}$, and $V = V_{ortho} = 2V_{hex}$ [32] represent the unit cell volume and lattice parameters of the two structures. The Mn-Mn moments are seen to have exchanges in interaction along the axis, indicated by the lattice parameter b . A change strongly influenced the Curie temperature in this parameter.

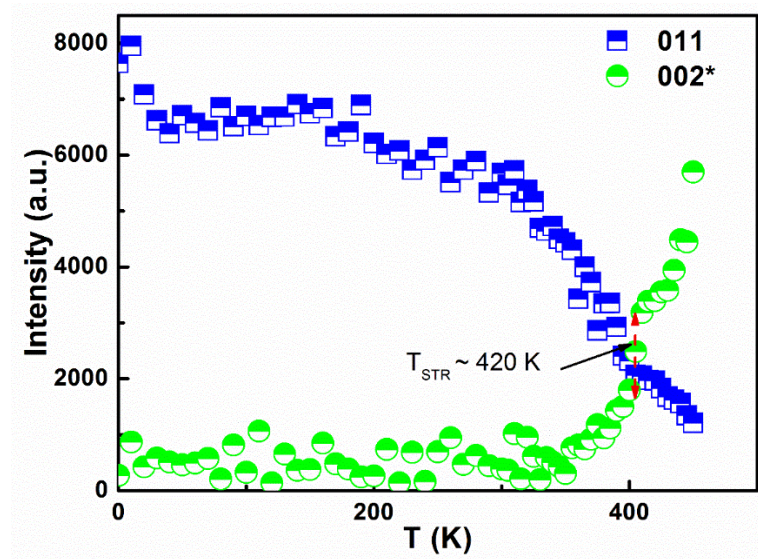


Figure 12. Temperature against the peak intensity for the (002)* and (011) peaks of the MnCoGe_{0.97}Al_{0.03} compound.

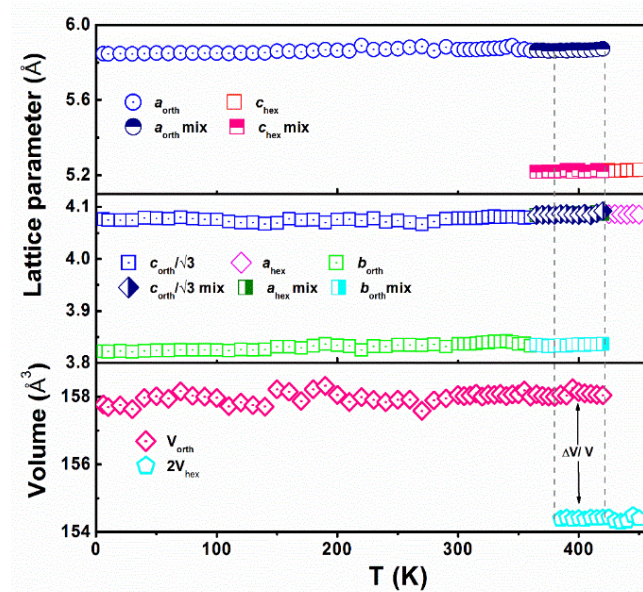


Figure 13. Temperature function in terms of lattice parameters and unit cell volume of MnCoGe_{0.97}Al_{0.03}. Open symbols with dots on the centre denote the orthorhombic phase, open symbols denote the hexagonal phase, and half-filled symbols denote the corresponding phases in the mixed phase region.

A large change of volume ($\Delta V = \frac{1}{2}V_{\text{orth}} - V_{\text{hex}} = 2.02 \text{ \AA}^3$, so $\Delta V/V \approx 2.35\%$) was detected at about the temperature of structural transition $T_{\text{str}} \approx 420 \text{ K}$ during the change of symmetry from hexagonal to orthorhombic. The MnCoGe compound was approximated based on its difference from Kanomata et al. [33] in the unit cell volume ($\Delta V \approx 3 \text{ \AA}^3$ at T_{str}) for comparison purposes. For magnetic phase transitions of the first order, the total field-induced magnetic entropy change, ΔS_{tot} , is defined as the total between the typical second-order magnetic entropy change (ΔS_{M}) and the two different crystallographic polymorphs' (ΔS_{st}) entropy difference, i.e., $\Delta S_{\text{tot}} = \Delta S_{\text{M}} + \Delta S_{\text{st}}$. The volume disparities between the transitional phases are proportional to the structural entropies. The volume difference around T_{str} for the MnCoGe_{0.97}Al_{0.03} compound caused structural entropy change, which resulted in total magnetic entropy change. The MCE around the T_{str} value (approximately $9 \text{ J kg}^{-1} \text{ K}^{-1}$ for $\Delta B = 5 \text{ T}$) is larger than at T_{C} ($4.92 \text{ J kg}^{-1} \text{ K}^{-1}$ for $\Delta B = 5 \text{ T}$) in the MnCoGe_{0.97}Al_{0.03} compound. This observation can be associated with the combined

effect of a sudden magnetization change and the change in unit cell volume in the proximity of structural entropy change (structural transition).

4. Conclusions

The Al replacement for Ge atoms has changed structural transformation at room temperature. The Al doping decreased the T_{str} at 450 to 420 K. The Mn-Mn covalent bonding strengthened with the decrease in T_{str} . Meanwhile, the Al doping reduced the c/a ratio. The magnetic transition found that with the Al doping, the T_c value slightly increased from 342 K to 352 K.

The analysis performed using the isothermal magnetization in the proximity of T_C agreed well with the critical exponents of the $\text{MnCoGe}_{0.97}\text{Al}_{0.03}$ compound. The Kouvel–Fisher method, critical isotherm analysis, and modified Arrott plots were among the different techniques on which the analysis was based. All the critical exponents fulfilled the Widom scaling law. The critical exponent that was evaluated had values that were near the mean values of the field theory with interactions that were long in range.

For $\text{MnCoGe}_{0.97}\text{Al}_{0.03}$, a change in the moderate magnetic entropy, $-\Delta S_M$, was identified to represent second-order magnetic transition behaviour. Magnetic refrigeration applications were favourable for temperature regions of 320 to 350 K. The Ge that Al substituted in the $\text{MnCoGe}_{0.97}\text{Al}_{0.03}$ compound caused the magnetic and structural transition separation.

Neutron diffraction signified that structural transition occurred with decreasing temperature around 430 K to 350 K. The substitution of Al for Ge enhanced the stability of the $P63/mmc$ hexagonal phase. The Rietveld refining method analysis showed that the lattice parameters and the volume phase fraction change ($\Delta V = 1/2V_{\text{orth}} - V_{\text{hex}} = 2.02 \text{ \AA}^3$, so $\Delta V/V \approx 2.35\%$) were detected at about the temperature of structural transition $T_{\text{str}} \approx 420 \text{ K}$ during the change of symmetry from hexagonal to orthorhombic. The structural entropies were proportional to the volume differences of the transition's phase, which resulted in total magnetic entropy change. Hence, it showed the combined effect of sudden magnetization changes and unit cell volume changes in the structural entropy change.

Author Contributions: A.R.A.R.: Writing—Original Draft, Visualization. M.F.M.D.: Writing—Review and Editing, Data Curation. J.W.: Conceptualization, Supervision. N.S.S.: Visualization. N.K.O.: Project administration. N.F.M.S.: Resources, data curation. S.X.D.: Resources, data curation. N.F.M.: Validation, Funding acquisition. All authors have read and agreed to the published version of the manuscript.

Funding: This work is supported in part by the Fundamental Research Grant Scheme (FRGS/1/2019/STG07/UPNM/02/7) from the Ministry of Higher Education Malaysia and National Defence University of Malaysia Grant Scheme (UPNM/2021/GPJP/TK/4).

Data Availability Statement: Not applicable.

Acknowledgments: The authors thank the National Defence University of Malaysia for the financial support of this research.

Conflicts of Interest: The authors declare no conflict of interest.

References

1. Gschneidner, K.A., Jr.; Pecharsky, V.K. Magnetocaloric materials. *Annu. Rev. Mater. Sci.* **2000**, *30*, 387–429. [[CrossRef](#)]
2. Weiss, P.; Piccard, A. Le phénomène magnétocalorique. *J. Phys. Theor. Appl.* **1917**, *7*, 103–109. [[CrossRef](#)]
3. Smith, A. Who discovered the magnetocaloric effect? *Eur. Phys. J. H* **2013**, *38*, 507–517. [[CrossRef](#)]
4. Zimm, C.; Jastrab, A.; Sternberg, A.; Pecharsky, V.; Gschneidner, K.; Osborne, M.; Anderson, I. Description and performance of a near-room temperature magnetic refrigerator. In *Advances in Cryogenic Engineering*; Springer: New York, NY, USA, 1998; pp. 1759–1766.
5. Brown, G.V. Magnetic heat pumping near room temperature. *J. Appl. Phys.* **1976**, *47*, 3673–3680. [[CrossRef](#)]
6. Nikitin, S.A.; Tishin, A.M.; Leontiev, P.I. Magnetocaloric effect and pressure influence on dysprosium single crystal magnetization in the range of magnetic phase transition. *J. Magn. Magn. Mater.* **1991**, *92*, 405–416. [[CrossRef](#)]

7. Dan'kov, S.Y.; Spichkin, Y.I.; Tishin, A.M. Magnetic entropy and phase transitions in Gd, Tb, Dy and Ho. *J. Magn. Magn. Mater.* **1996**, *152*, 208–212. [[CrossRef](#)]
8. Coey, J.M.D.; Skumryev, V.; Gallagher, K. Is gadolinium really ferromagnetic? *Nature* **1999**, *401*, 35–36. [[CrossRef](#)]
9. Rahman, A.R.A.; Din, M.F.M.D.; Hairudin, N.A.; Suhaimi, N.S.; Wang, J.; Tawil, S.N.M.; Ismail, M.; Idris, N.H. Effect of Ball Milling Methods on Structural and Electrical Properties of La (FeSi) 13 Alloys. *Des. Eng.* **2021**, *7*, 12984–12989.
10. Phan, M.-H.H.; Yu, S.-C.C. Review of the magnetocaloric effect in manganite materials. *J. Magn. Magn. Mater.* **2007**, *308*, 325–340. [[CrossRef](#)]
11. Bingham, N.S.; Phan, M.H.; Srikanth, H.; Torija, M.A.; Leighton, C. Magnetocaloric effect and refrigerant capacity in charge-ordered manganites. *J. Appl. Phys.* **2009**, *106*, 23909. [[CrossRef](#)]
12. Moya, X.; Hueso, L.E.; Maccherozzi, F.; Tovstolytkin, A.I.; Podyalovskii, D.I.; Ducati, C.; Phillips, L.C.; Ghidini, M.; Hovorka, O.; Berger, A. Giant and reversible extrinsic magnetocaloric effects in $\text{La}_{0.7}\text{Ca}_{0.3}\text{MnO}_3$ films due to strain. *Nat. Mater.* **2013**, *12*, 52–58. [[CrossRef](#)] [[PubMed](#)]
13. Zeng, R.; Dou, S.X.; Wang, J.L.; Campbell, S.J. Large magnetocaloric effect in re-entrant ferromagnet $\text{PrMn}_{1.4}\text{Fe}_{0.6}\text{Ge}_2$. *J. Alloys Compd.* **2011**, *509*, L119–L123. [[CrossRef](#)]
14. Wang, J.L.; Campbell, S.J.; Md Din, M.F.; Kennedy, S.J.; Hofmann, M. Magnetic transitions and the magnetocaloric effect in the $\text{Pr}_{1-x}\text{Y}_x\text{Mn}_2\text{Ge}_2$ system. *Phys. Status Solidi* **2014**, *211*, 1092–1100. [[CrossRef](#)]
15. Dou, S.X.; Wang, J.; Zeng, R.; Poh, C.-K.; Campbell, S.J.; Kennedy, S.J. Re-entrant ferromagnet $\text{PrMn}_2\text{Ge}_{0.8}\text{Si}_{1.2}$: Magnetocaloric effect. *J. Appl. Phys.* **2009**, *105*, 07A909.
16. Wang, J.L.; Caron, L.; Campbell, S.J.; Kennedy, S.J.; Hofmann, M.; Cheng, Z.X.; Din, M.F.M.; Studer, A.J.; Brück, E.; Dou, S.X. Driving magnetostructural transitions in layered intermetallic compounds. *Phys. Rev. Lett.* **2013**, *110*, 217211. [[CrossRef](#)]
17. Devarajan, U.; Nair, S. Investigations on Cu induced couple-decoupled magneto-structural transition in MnCoGe alloys. *Mater. Res. Express* **2019**, *6*, 106117. [[CrossRef](#)]
18. Liu, J.; You, Y.; Batashev, I.; Gong, Y.; You, X.; Huang, B.; Zhang, F.; Miao, X.; Xu, F.; van Dijk, N.; et al. Design of Reversible Low-Field Magnetocaloric Effect at Room Temperature in Hexagonal MnMX Ferromagnets. *Phys. Rev. Appl.* **2020**, *13*, 054003. [[CrossRef](#)]
19. Si, X.; Zhou, K.; Zhang, R.; Qi, J.; Liu, Y. Room-temperature magnetocaloric properties and universal curve of $\text{MnCo}_{1-x}\text{Sn}_x\text{Ge}$. *Phys. Lett. Sect. A Gen. At. Solid State Phys.* **2017**, *381*, 2850–2855. [[CrossRef](#)]
20. Gao, T.; Wu, M.; Qi, N.; Zhou, T.; Luo, X.; Liu, Y.; Xu, K.; Marchenkov, V.V.; Dong, H.; Chen, Z.; et al. Giant low field magnetocaloric effect and magnetostructural coupling in $\text{MnCoGe}_{1-x}\text{In}_x$ around room temperature. *J. Alloys Compd.* **2018**, *753*, 149–154. [[CrossRef](#)]
21. Rahman, A.R.A.; Md Din, M.F.; Wang, J.; Suhaimi, N.S.; Idris, N.H.; Dou, S.X.; Ismail, M.; Hassan, M.Z.; Jusoh, M.T. Magnetism and Thermomechanical Properties in Si Substituted MnCoGe Compounds. *Crystals* **2021**, *11*, 694. [[CrossRef](#)]
22. Bao, L.F.; Hu, F.X.; Wu, R.R.; Wang, J.; Chen, L.; Sun, J.R.; Shen, B.G.; Li, L.; Zhang, B.; Zhang, X.X. Evolution of magnetostructural transition and magnetocaloric effect with Al doping in $\text{MnCoGe}_{1-x}\text{Al}_x$ compounds. *J. Phys. D Appl. Phys.* **2014**, *47*, 055003. [[CrossRef](#)]
23. Arrott, A.; Noakes, J.E. Approximate equation of state for nickel near its critical temperature. *Phys. Rev. Lett.* **1967**, *19*, 786. [[CrossRef](#)]
24. Ren, Q.Y.; Hutchison, W.D.; Wang, J.L.; Pérez, S.M.; Cadogan, J.M.; Campbell, S.J. Magnetism and magnetocaloric effect of $\text{Mn}_{0.98}\text{Fe}_{0.02}\text{CoGe}$. *Phys. Status Solidi Appl. Mater. Sci.* **2014**, *211*, 1101–1105. [[CrossRef](#)]
25. Banerjee, B.K. On a generalised approach to first and second order magnetic transitions. *Phys. Lett.* **1964**, *12*, 16–17. [[CrossRef](#)]
26. Sahana, M.; Rössler, U.K.; Ghosh, N.; Elizabeth, S.; Bhat, H.L.; Dörr, K.; Eckert, D.; Wolf, M.; Müller, K.-H. Critical properties of the double-exchange ferromagnet $\text{Nd}_{0.6}\text{Pb}_{0.4}\text{MnO}_3$. *Phys. Rev. B* **2003**, *68*, 144408. [[CrossRef](#)]
27. Kouvel, J.S.; Fisher, M.E. Detailed Magnetic Behavior of Nickel Near its Curie Point. *Phys. Rev.* **1964**, *136*, A1626–A1632. [[CrossRef](#)]
28. Ahlberg, M.; Korelis, P.; Andersson, G.; Hjörvarsson, B. Effect of ferromagnetic proximity on critical behavior. *Phys. Rev. B* **2012**, *85*, 224425. [[CrossRef](#)]
29. Franco, V.; Conde, A.; Romero-Enrique, J.M.; Blázquez, J.S. A universal curve for the magnetocaloric effect: An analysis based on scaling relations. *J. Phys. Condens. Matter* **2008**, *20*, 285207. [[CrossRef](#)]
30. Md Din, M.F.; Wang, J.L.; Campbell, S.J.; Studer, A.J.; Avdeev, M.; Kennedy, S.J.; Gu, Q.F.; Zeng, R.; Dou, S.X. Magnetic phase transitions and entropy change in layered $\text{NdMn}_{1.7}\text{Cr}_{0.3}\text{Si}_2$. *Appl. Phys. Lett.* **2014**, *104*, 42401. [[CrossRef](#)]
31. Caron, L.; Ou, Z.Q.; Nguyen, T.T.; Thanh, D.T.C.; Tegus, O.; Brück, E.; Cam Thanh, D.T.; Tegus, O.; Brück, E. On the determination of the magnetic entropy change in materials with first-order transitions. *J. Magn. Magn. Mater.* **2009**, *321*, 3559–3566. [[CrossRef](#)]
32. Wang, J.-T.; Wang, D.-S.; Chen, C.; Nashima, O.; Kanomata, T.; Mizuseki, H.; Kawazoe, Y. Vacancy induced structural and magnetic transition in $\text{MnCo}_{1-x}\text{Ge}$. *Appl. Phys. Lett.* **2006**, *89*, 262504. [[CrossRef](#)]
33. Kanomata, T.; Ishigaki, H.; Suzuki, T.; Yoshida, H.; Abe, S.; Kaneko, T. Magneto-volume effect of $\text{MnCo}_{1-x}\text{Ge}_{(0 \leq x \leq 0.2)}$. *J. Magn. Magn. Mater.* **1995**, *140–144*, 131–132. [[CrossRef](#)]